Ann. Geophys., 24, 823–834, 2006
www.ann-geophys.net/24/823/2006/
© European Geosciences Union 2006

Annales Geophysicae

Lidar observations of middle atmospheric gravity wave activity over a low-latitude site (Gadanki, 13.5° N, 79.2° E)

V. Sivakumar[1,2], **P. B. Rao**[3], **and H. Bencherif**[1]

[1]Laboratoire de l'Atmosphère et des Cyclones, CNRS–UMR 8105, Université de La Réunion, 97715 Saint-Denis Messag. Cedex 9, La Reunion, France
[2]Initially at National Atmospheric Research Laboratory, Gadanki-517 502, India
[3]National Remote Sensing Agency, Bala Nagar, Hyderabad-500 037, India

Received: 28 July 2005 – Revised: 17 February 2006 – Accepted: 28 February 2006 – Published: 19 May 2006

Abstract. The low-latitude middle atmospheric gravity wave characteristics are presented using 310 nights of Rayleigh lidar observations made at Gadanki (13.5° N, 79.2° E) over the period from March 1998 to December 2002. The gravity wave characteristics are presented in terms of vertical wave number and frequency spectra, along with the estimated potential energy for the four seasons, namely, spring, summer, autumn and winter. The computed wave number spectra for both the stratosphere and the mesosphere are found to differ significantly from a saturated model predicted spectrum. The spectra were found to be shallower at lower wave numbers and steeper at higher wave numbers with transition at $\sim 8.85 \times 10^{-4}$ cy/m. The computed frequency spectra seem to follow the model plot with a power law index of –5/3 above a frequency of $\sim 2 \times 10^{-4}$ Hz. The estimated potential energy per unit mass increases gradually up to ∼60 km and then rather rapidly above this height to reach values of the order of 200 J/kg at ∼70 km.

Keywords. Atmospheric composition and structure (Pressure, density and temperature; Middle atmosphere – composition and chemistry) – Meteorology and atmospheric dynamics (Middle atmosphere dynamics; Waves and tides)

1 Introduction

Gravity waves (GW) play a major role in transporting momentum and energy from the lower atmosphere to the upper atmosphere. These waves, having their source at lower heights, propagate upwards and deposit energy through wave breaking and dissipation processes in the mesosphere, thereby significantly altering its thermal structure and wind pattern (Booker and Bretherton, 1967; Lindzen, 1973; Dunkerton, 1982; McIntyre, 1980; Fritts, 1984; Fritts and Rastogi, 1985; Whiteway and Carswell, 1995; Nastrom et al., 1997; Gavrilov et al., 2000; Nastrom and vanZandt, 2001; Fritts and Alexander, 2003). The GW thus have a significant impact on the dynamical processes in the middle atmosphere. It is believed that convective instabilities occurring in the lower atmosphere act as a major source for the generation of GW (e.g. Fritts, 1984; Fritts and Rastogi, 1985) with the convective phenomena being dominant in the tropical region, it is of considerable significance to study GW activity over the tropics.

There have been a number of observational studies on GW in the middle atmosphere using various techniques (e.g. Röttger, 1980; Vincent, 1984; Wilson et al., 1991a, b; Namboothiri et al., 1996; Alexander et al., 2002; Fritts and Alexander, 2003). In recent years, the Rayleigh lidar technique has emerged as an effective means to study the GW activity in the middle atmosphere over the height range of 30–70 km. However, most of the GW studies by the lidar technique over the past two decades have been confined to the high and mid latitudes (Chanin and Hauchecorne, 1981, 1991; Wilson et al., 1991a, b; Gardner et al., 1989; Marsh et al., 1991; Mitchell et al., 1991; Beatty et al., 1992; Whiteway and Carswell, 1995; McDonald et al., 1998; Fritts and Alexander, 2003). Using the lidar observations made from two stations, Haute Provence (44° N, 6° E) and Biscarrosse (44° N, 1° W), Chanin and Hauchecorne (1981, 1991) and Wilson et al. (1991a, b) have made detailed studies on GW activity in the middle atmosphere over the south of France. They found the GW activity maximum during winter and minimum during summer. The dominant wave periods range from 6 to 8 h and vertical wavelengths from 5 to 10 km. They have noted wave saturation taking place around 60 km. The GW associated potential energy estimates have shown significant seasonal dependence for both the stations. The lidar observations over Arecibo (18° N, 66° W) reported by Beatty et al. (1992) have shown increasing GW amplitude with increasing wave period and vertical wavelength. The

Correspondence to: V. Sivakumar
(siva@univ-reunion.fr)

Published by Copernicus GmbH on behalf of the European Geosciences Union.

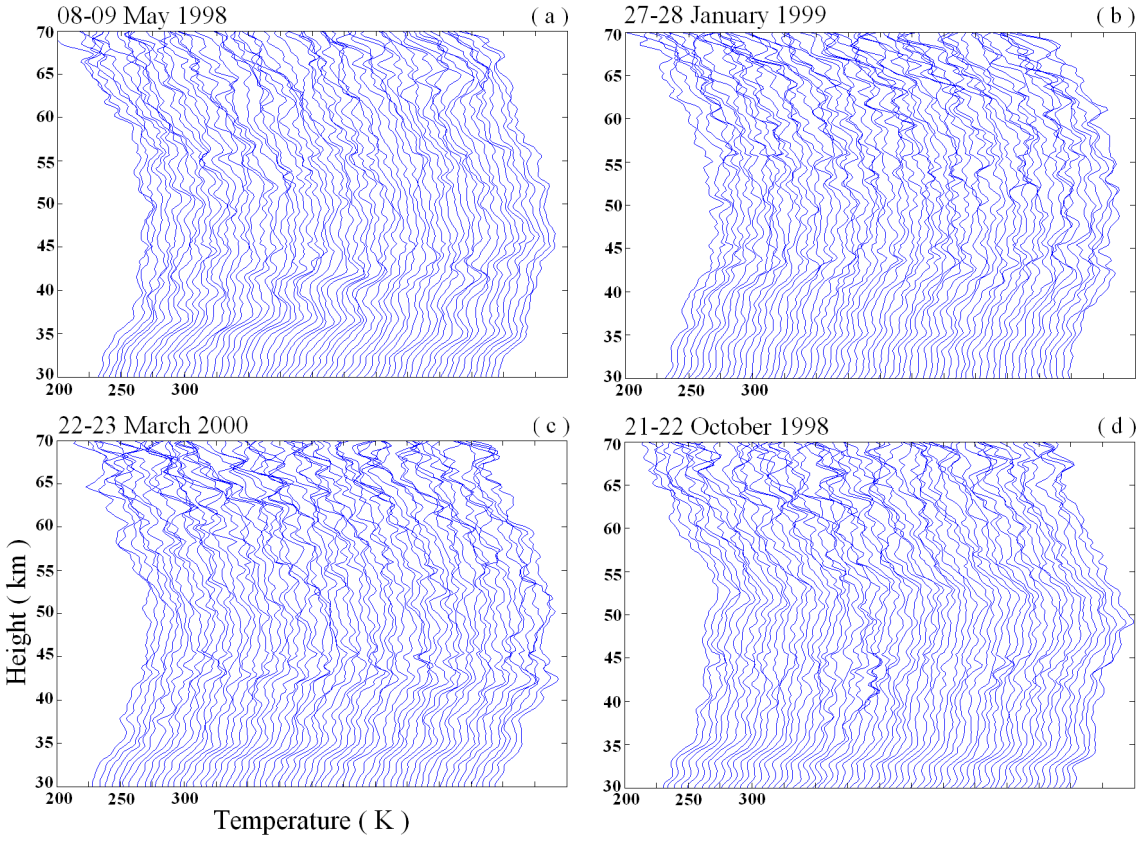

Fig. 1. A time sequence of 64 temperature profiles observed on the nights of 8–9 May 1998, 27–28 January 1999, 22–23 March 2000 and 21–22 October 1998. The successive profiles are offset by 5 K.

wave periods were found to be in the range from 1 1/2 to 15 h and vertical wavelengths in the range of 1–17 km. The lidar observations of the GW characteristics over Urbana (40° N, 88° W) were found to be similar to those reported for Arecibo (Gardner et al., 1989). The lidar observations made over Toronto (44° N, 80° W) have shown that the GW activity is maximum during winter and minimum during summer (Whiteway and Carswell, 1995), same as observed over south of France. The effective growth rates of the gravity waves were found to be less than that required based on the consideration of energy conservation. They have also reported significant day-to-day variability in the wave-associated potential energy. McDonald et al. (1998) made observations on GW activity using the lidar and MST radar systems at Aberystwyth (52.4° N, 4.1° W) and Valentia (51.9° N, 10.2° W). They found that the gravity waves vary from night-to-night and have wave periods ranging from 6 to 17 h and vertical wavelengths of the order of 10 km. The convective instabilities were shown to be the cause for the observed gravity waves. Using MU radar observations over Shigaraki (35° N, 136° E), Fritts et al. (1990) found that the mean vertical profiles of energy density show with height a decaying trend at low frequencies and a growing trend at higher frequencies. Further, Gavrilov et al. (2000) have made a detailed study on GW characteristics and momentum fluxes in the mesosphere and found that at these heights, GW breaking takes place and as a consequence turbulence is generated. Recently, Fritts and Alexanader (2003) have reviewed the gravity wave activity in the middle atmosphere and established that the waves with vertical wavelengths greater than 10 km are generally considered to be important in the middle-atmosphere dynamics and such long vertical wavelengths ($>$10 km) are associated with deep convective heating. They also pointed out that the wave amplitudes can grow up to the mesospheric heights with large intrinsic phase speeds and wave breaking or dissipation tends to occur only as waves approach their critical levels. There have not been many studies similar to the above on gravity waves in the middle atmosphere for low latitudes. The present study aims at delineating the GW characteristics in the middle atmosphere using the Rayleigh lidar observations made at Gadanki (13.5° N, 79.2° E). The results include GW characteristics related to their growth, saturation and the associated potential energy.

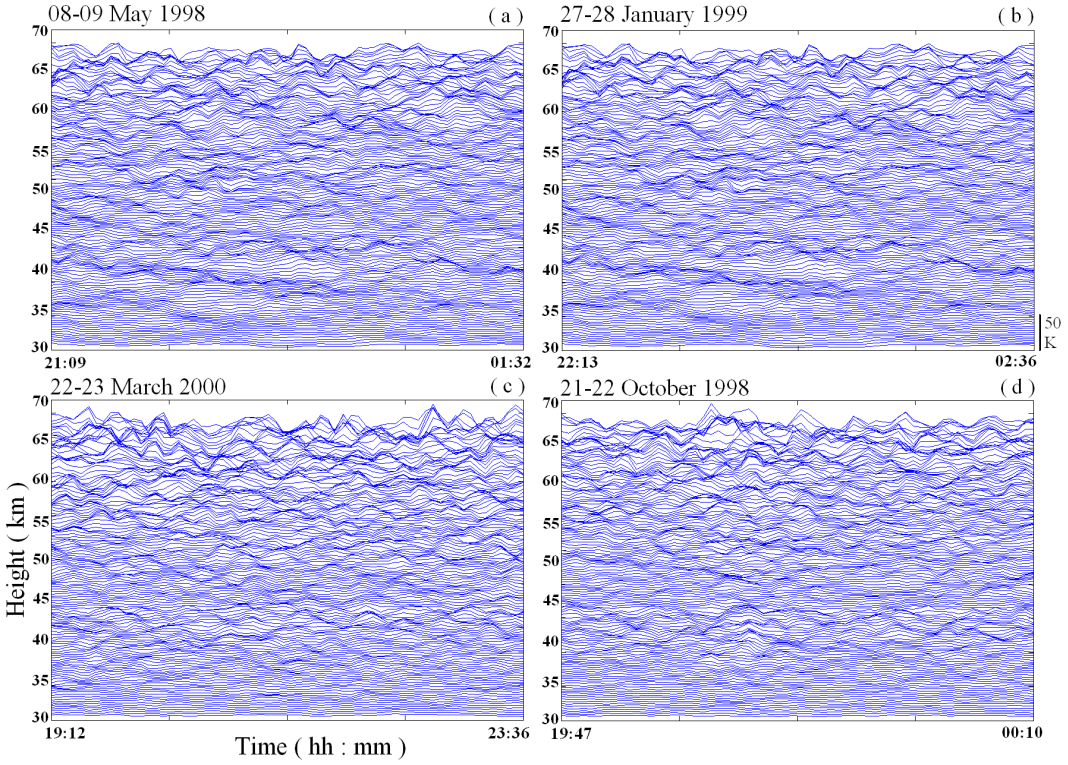

Fig. 2. Height-time variations of temperature fluctuations T′ obtained by removing the linear temporal trend at each height for the same days as in Fig. 1.

2 Data and analysis

The lidar observations presented here were made on 310 nights during the period from March 1998 to December 2002. The data were collected continuously for a period of 4 to 6 h on clear nights, starting around 20:00 LT. The recorded raw data is in the form of photon count profiles with a height resolution of 300 m and time resolution of 250 s (5000 laser shots were integrated for one profile). The height range considered for the present study extends from 30 to 70 km, although the temperature was derived up to 90 km. The large fluctuations resulting from a low signal-to-noise ratio at higher heights is the reason for limiting the height coverage to 70 km for wave studies. The method of deriving the temperature profile from the measured photon count profile closely follows the method given by Hauchecorne and Chanin (1980) and is described in detail by Sivakumar et al. (2003). The time duration and height extent of the data determine the upper limits of the wave period and vertical wavelength, respectively. The data frames used for the spectral analysis are of ∼4 1/2 h duration and 19.2 km in height extent (64 sample points in both cases). It may be noted that for computing the wave number and frequency spectra, the total height range (30–70 km) is divided into two blocks, one covering the stratosphere height range of 30–50 km and the other the mesosphere height range of 50–70 km. It is assumed that the GW induced density perturbations are similar to those of temperature (Whiteway and Carswell, 1994, 1995; Namboothiri et al., 1996).

The temperature perturbations, from which the vertical wave number spectra are derived, are extracted by subtracting from the height profile of the temperature a third order polynomial fit applied to the entire height range. In the case of frequency spectra, the temperature perturbations are obtained by removing a linear trend and applying a windowing technique to remove the long-term trend from the time series of the temperature data for a given altitude level. The adaptive filter method is used to remove the noise in the power spectral density by employing hanning window with 95% of confidence level. Therefore the spectral results are better in accuracy and free from noise. For the vertical wave number spectra, following Wilson et al. (1991a), the perturbations are defined as $\left(\frac{g}{N^2}\right)\left(\frac{T'}{T_0}\right)$ in order to be able to make a comparison with the saturation spectral limit, independent of the mean static stability and temperature conditions. In the above expression, g is the acceleration due to gravity, N is the Brunt Väisälä frequency, T_0 and T' are the mean temperature and temperature perturbation, respectively; N is computed using the expression:

$$N^2 = \frac{g}{T_p}\left[\frac{dT_p}{dz} + \Gamma\right]. \quad (1)$$

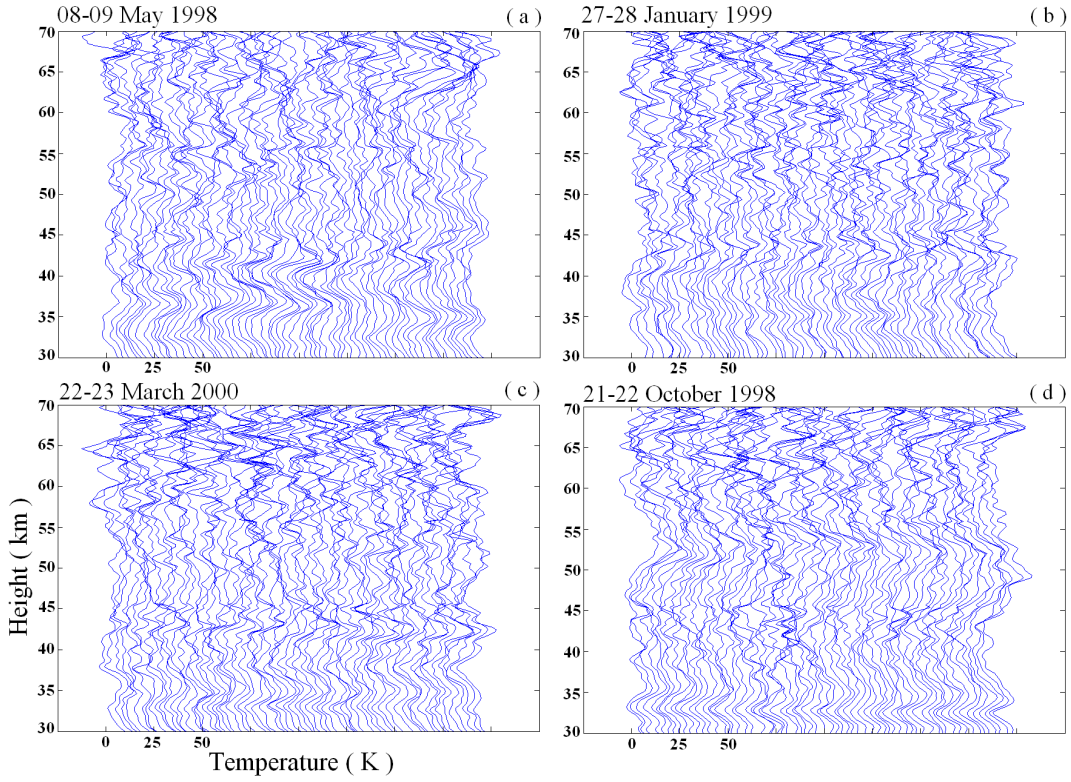

Fig. 3. A time sequence of 64 vertical profiles of temperature fluctuations obtained by subtracting the third order polynomial fit from the observed temperature profiles for the same days as in Fig. 1. The successive profiles are offset by 3 K.

Where, "Γ" is the adiabatic lapse rate (= –9.8./km), and T_p is the temperature value taken from the 3rd order polynomial fit applied to the mean temperature profile.

In the case of frequency spectra, the perturbations are defined as $\left(\frac{g}{N}\right)\left(\frac{T'}{T_0}\right)$ and their variance turns out to be twice the potential energy. In the present study, the wave number and the frequency spectra, as well as the height profiles of potential energy, were computed for the four seasons – summer, winter, spring equinox and autumn equinox, which correspond to the months of May to August, November to February, March to April and September to October, respectively.

3 Observations

In this section, we present the method of extraction of GW perturbation profiles and their frequency and wave number spectra for four representative days, one each in summer, winter, spring and autumn. The basic features of low-latitude GW are brought out from these case studies. The following section (Sect. 4), authenticating the case study results, presents the seasonal mean plots of frequency and wave number spectra, as well as height profiles of potential energy.

3.1 Height-time profiles of temperature and its perturbations

A time sequence of 64 temperature profiles at a 250-s interval, covering a height range of 30-70 km, is presented in Figs. 1a–d for the nights of 8–9 May 1998, 27–28 January 1999, 22–23 March 2000 and 21–22 October 1998. The profiles clearly reveal wave perturbations in temperature for all four sets. The wave perturbations are characterized by downward phase progression, as expected for upward propagating gravity waves. The rate of progression, which is clearly seen for lower heights (<50 km), is found to be in the range of ∼0.15–0.3 m/s. On the basis of vertical wavelengths associated with these perturbations, it can be inferred that they correspond to wave periods (∼7 h.) larger than the observational time period. The height-time variations of the temperature fluctuations, obtained by removing a linear temporal trend at each height, are presented for the same four days in Figs. 2a–d. It may be noted that these fluctuations are due to waves with periods less than the observational period, since the detrending of the data effectively removed the contribution due to longer periods. The wave amplitudes associated with the fluctuations are found to increase with height in all four cases. The perturbation amplitudes are of the order of 10–20 K in the mesosphere and considerably lower (∼5–

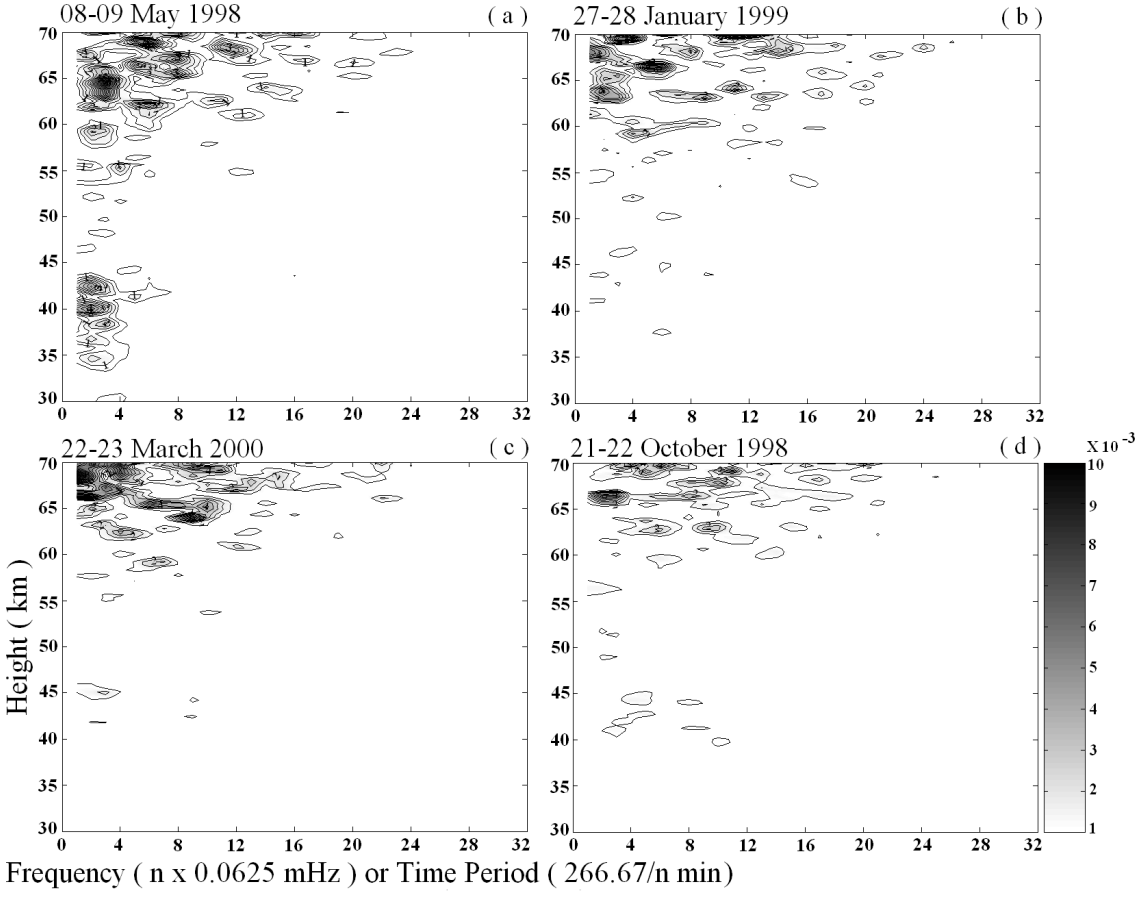

Fig. 4. Frequency–power spectra of relative temperature fluctuation as a function of height for the cases shown in Fig. 2.

10 K) in the stratosphere. The wave perturbations, seen more clearly in the case of 8–9 May 1998, are found to have periodicities of the order of 30–40 min. The variance of the fluctuations $\left\langle \left(\Delta T'\right)^2 \right\rangle$ representing the intensity of the wave activity, averaged over the height range 60–70 km, is found to be maximum (49.1 K^2) for 22–23 March 2000 and minimum (22.0 K^2) for 21–22 October 1998. Figures 3a–d show for the same cases a time sequence of 64 vertical profiles of temperature perturbation derived by subtracting the third order polynomial fit from the observed temperature profiles. The dominant perturbations seen at lower heights (<50 km) with low rates of downward phase progression are clearly due to longer period waves mentioned earlier. The vertical wavelengths of these waves appear to be of the order of 5–10 km. For the downward phase progression of ∼0.15-0.3 m/s, the wave period would be of the order of ∼7 h. The wave amplitudes associated with these waves are of the order of 10–15 K. The perturbations in the mesosphere are also of the same order, but these are due to contributions from shorter period gravity waves. Due to fast changes associated with the short wave period, the phase progression in the mesosphere cannot be seen so clearly as in the stratosphere.

3.2 GW spectral characteristics

The frequency and wave number power spectra are computed using the time and height series of the detrended relative temperature fluctuations, respectively. The frequency-power spectra for the four days, 8–9 May 1998, 27–28 January 1999, 22–23 March 2000 and 21–22 October 1998, are presented in Figs. 4a–d. The wave activity is clearly visible with the wave periods ranging 266 min to 20 min. For all four days, the wave activity is the highest at mesosphere heights, with significant wave periods covering the range from 20 min to 4 1/2 h. The GW activity is found to be most intense during 22–23 March 2000, with the most dominant mode having a period of ∼4 1/2 h and a PSD value about three times that of the other days. The stratosphere shows considerably lesser wave activity than the mesosphere, except for the day 8–9 May 1998 on which the stratosphere also reveals significant wave activity, with wave periods ranging from 66 min to 266 min.

The wave number power spectra for the same four days as the frequency spectra are presented in Figs. 5a–d. The dominant components have vertical wavelengths in the range of about ∼5–38 km. The temporal variation of wave number

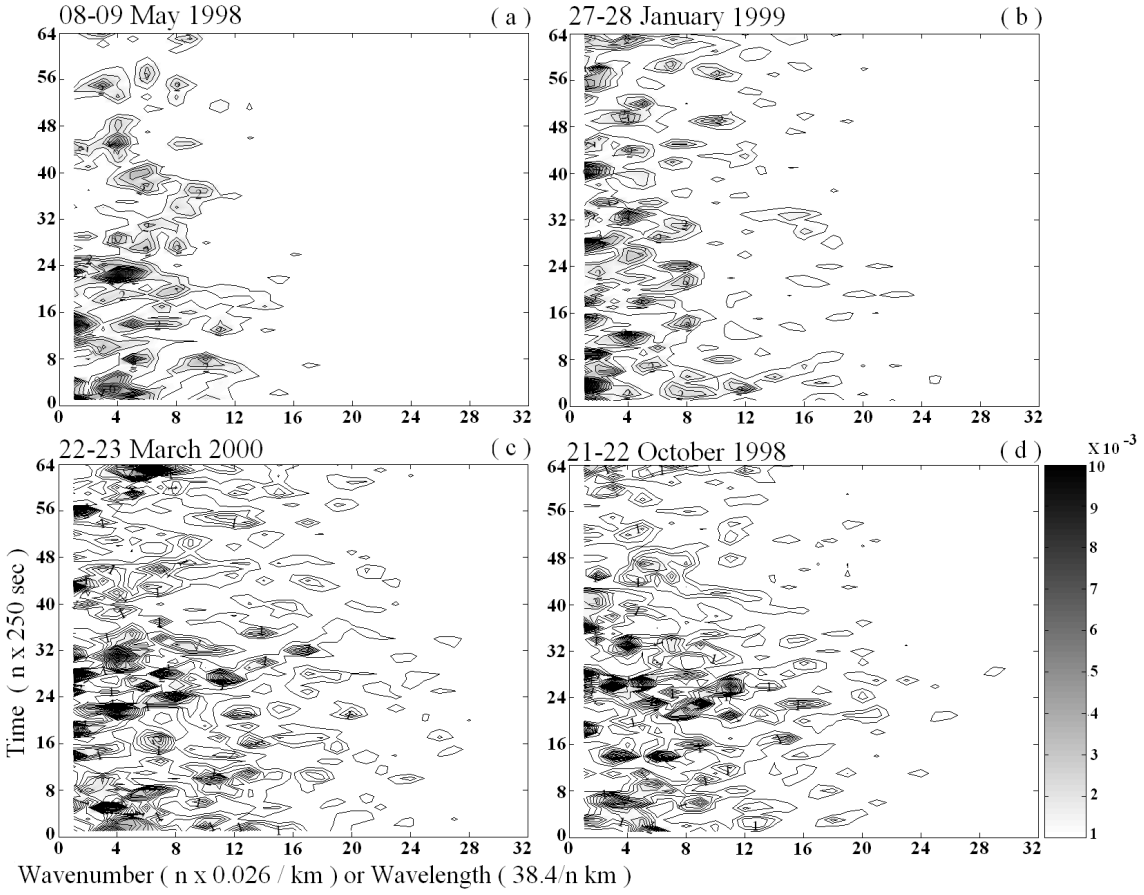

Fig. 5. Vertical wavenumber–power spectra for the 64 vertical profiles of relative temperature fluctuation for the cases shown in Fig. 3.

spectra for equinoctial days (22–23 March 2000 and 21–22 October 1998) shows significant variability for the entire period of observation (∼4 min to 4 1/2 h), with a wavelength ranging from ∼2.4 to 38.4 km. The other two days, 8–9 May 1998 (summer) and 27–28 January 1999 (winter), however, show the significant wavelength range to be ∼4.8 to 38.4 km and that the wave activity became with time, particularly for the summer day. The most dominant component with a wavelength of about 20–30 km is observed during the equinoctial day of 21–22 October 1998. As discussed above on the basis of Fig. 3, the modes with vertical wavelengths greater than 5 km correspond to longer period waves (>4 1/2 h). These modes with a low rate of vertical phase propagation are seen clearly at stratosphere heights and are referred to as quasi-stationary modes (Wilson et al., 1991a). The basic characteristics of these modes are found to be similar to that observed over midlatitudes (Gardner et al., 1989; Wilson et al., 1991a, b; Beatty et al., 1992).

4 Results and discussion

In this section, the above presented analysis is repeated for a given number of days for each season, to provide the seasonal features and examine the results obtained from the point of view of the above case studies. Although there are 310 nights of lidar observations over the site, we have limited the data used for studying the climatological characteristics to 52 days, with the distribution of 11, 24, 13 and 4 days during summer, winter, spring and autumn, respectively. The data quality, as assessed from the temporal consistency of the temperature profiles, and data continuity for periods exceeding 5 h, formed the basis in the selection of the above set of days. The results are represented in terms of the estimated GW associated potential energy (PE), seasonal mean frequency and wave number spectra and their comparison with the model spectra. The spectra illustrate the propagation and saturation characteristics of the GW modes.

4.1 Seasonal mean spectra and comparison with model

In order to study the saturation characteristics of the GW spectra, the vertical wave number spectra for stratosphere

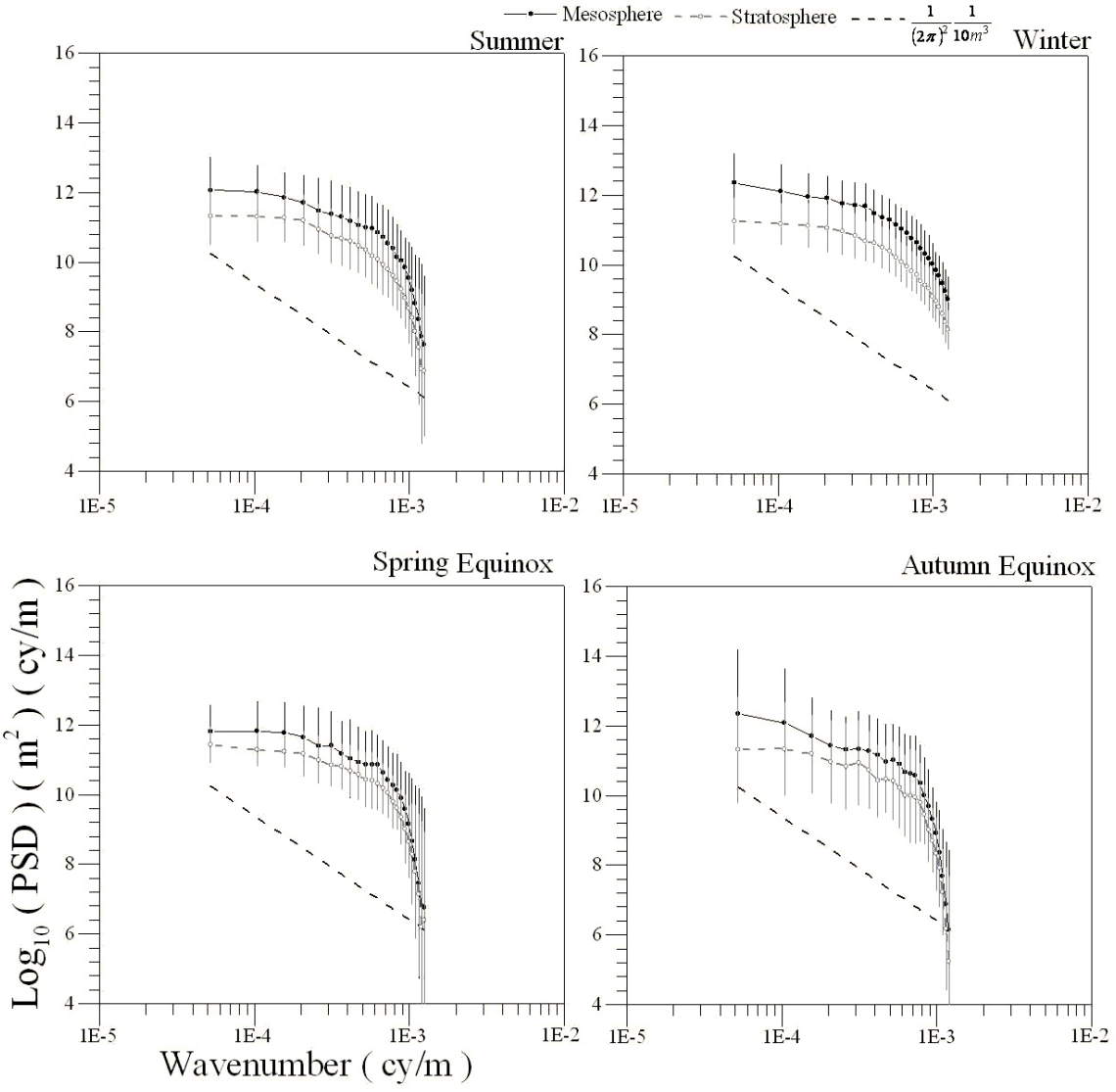

Fig. 6. Power spectral density versus vertical wave number of the relative temperature fluctuations scaled by g/N^2 for the mesosphere and stratosphere. A dashed line with slope of $\frac{1}{(2\pi)^2}\frac{1}{10m^3}$ representing saturation spectrum is also plotted for comparison.

and mesosphere are computed for relative temperature fluctuations scaled by $\frac{g}{N^2}$, following Wilson et al. (1991a). Using the dimensional analysis, Dewan and Good (1986) showed that the convective saturation of the wave motions lead to a vertical wave number spectrum of the form:

$$P^s(\mathrm{m}) = \alpha \frac{\mathrm{N}^4}{\mathrm{g}^2\mathrm{m}^3} \tag{2}$$

where $P^s(m)$ is the power spectral density for the saturated wave number (m).

More recently, following the method of Smith et al. (1987) for the saturation limit, the vertical wave number spectrum for the higher wave number "tail" region is expressed as (Allen and Vincent, 1995):

$$P^s(m) \approx \frac{N^4}{6g^2}\frac{1}{p}\frac{1}{(2\pi)^2}\frac{1}{m^3}\,. \tag{3}$$

Taking the 1-D frequency spectrum to be of the form $B(\omega)=B_0\omega^{-p}$ and the best estimate of "p" to be 5/3 (Allen and Vincent, 1995), Eq. (2) can be written as:

$$P^s(m) = \frac{N^4}{g^2}\frac{1}{(2\pi)^2}\frac{1}{10m^3}\,. \tag{4}$$

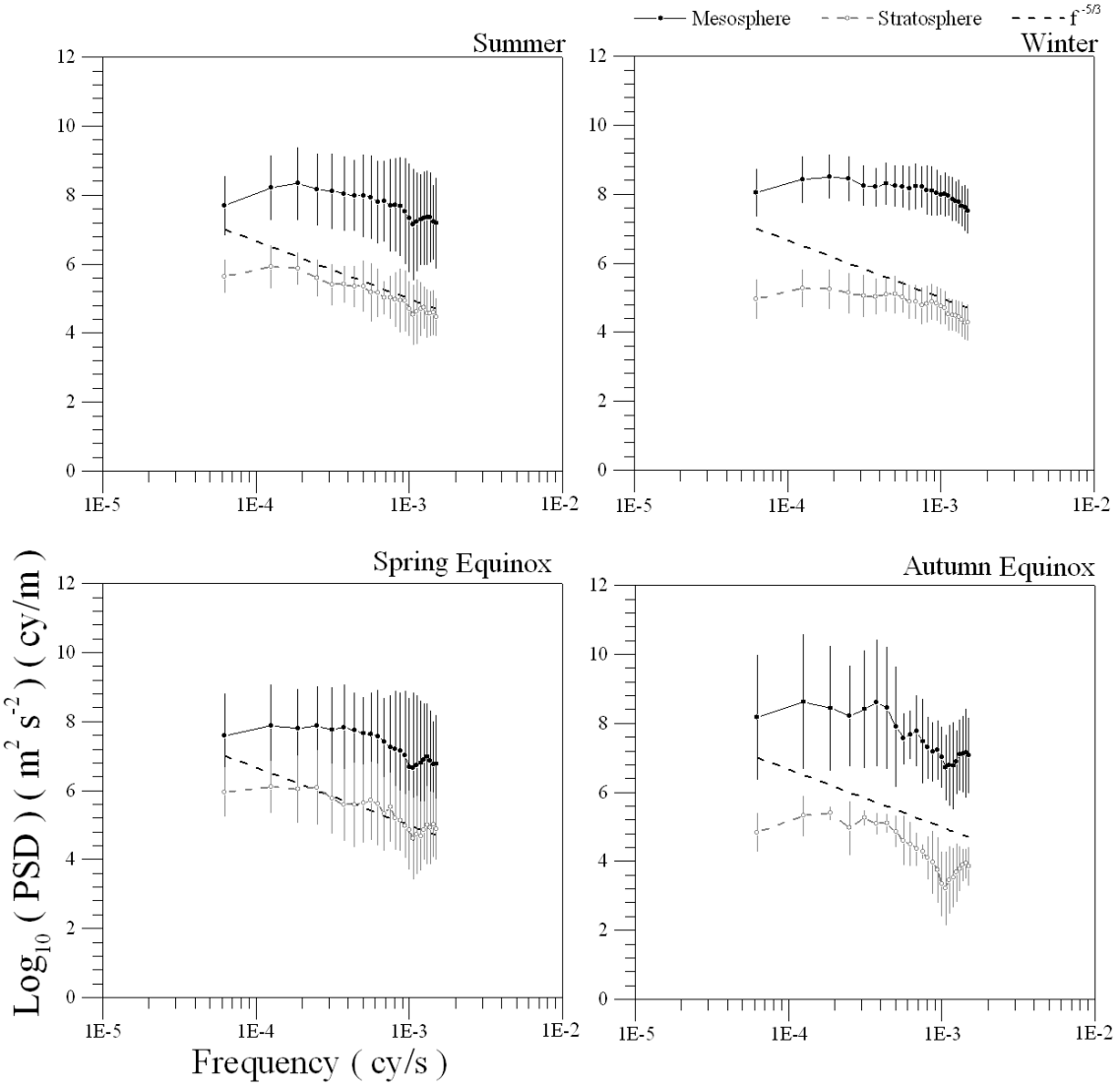

Fig. 7. Power spectral density versus frequency of the normalized temperature fluctuations for mesosphere and stratosphere. The dashed line with power law index of –5/3 is also plotted for comparison.

The power spectral density for the normalized temperature fluctuations weighted by $\frac{g}{N^2}$ takes the form:

$$P^{s\omega}(m) = \frac{1}{(2\pi)^2}\frac{1}{10m^3}. \quad (5)$$

Compare this with Eq. (2), $\alpha = \left(\frac{1}{40\pi^2}\right)$.

The wave number spectra were computed for all the selected days by performing FFT on the relative temperature fluctuations scaled by g/N^2. The spectra for each season were averaged and the seasonal average spectra, along with their standard deviations, are presented in Figs. 6a–d. The saturation spectrum model $\left(\frac{\alpha}{m^3}\right)$ is also shown in the figures for comparison. The computed spectra are found to differ from the model spectrum quite significantly, both in shape and magnitude. Compared to the model spectrum, the computed spectra are shallower at lower wave numbers and steeper at higher wave numbers, with the transition at $\sim 8.85\times10^{-4}$ cy/m. In magnitude, the computed spectra are greater by one to two orders of magnitude. The spectra for the stratosphere and mesosphere are found to be quite similar, with somewhat higher PSD values for the mesosphere. The spectra presented here for the low latitude are found to be generally in good agreement with that reported for mid-latitudes (Wilson et al., 1991a; Smith et al., 1987; Fritts et al., 1988; Tsuda et al., 1989; Wu and Widdel, 1989; 1991). The vertical wave number spectra computed for the lower atmosphere, using high resolution radiosonde measurements, showed that they remain approximately invariant with time and geographic location (Allen and Vincent, 1995). The

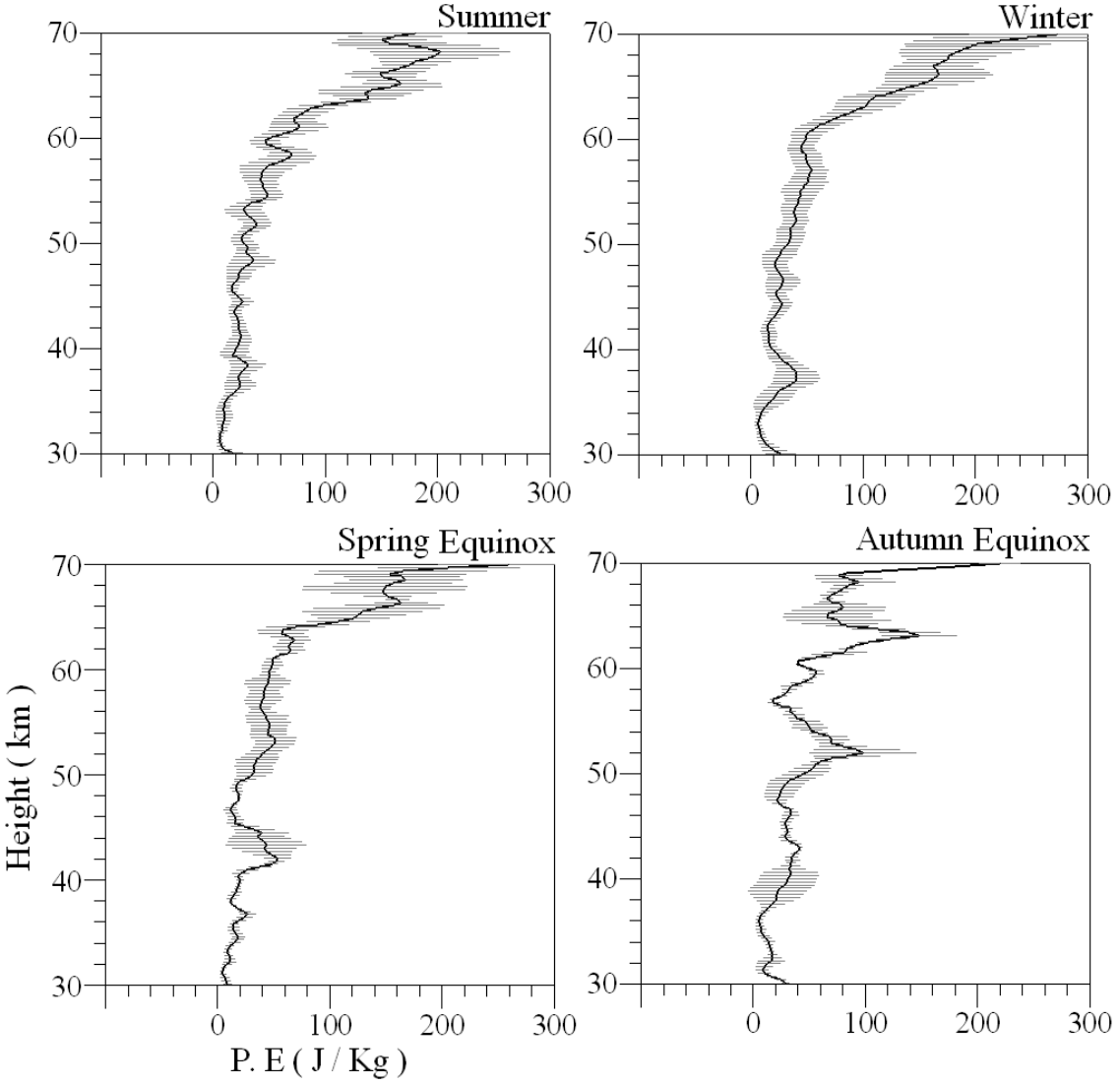

Fig. 8. Height profiles of seasonal mean potential energy per unit mass associated with the GW perturbations for the four different seasons.

kind of differences noted here between the observed and the model spectra have also been reported earlier by Nastrom et al. (1997) for the troposphere and stratosphere using balloon ascents over central Illinois.

Using the time series of the relative temperature fluctuations weighted by $\left(\frac{g}{N}\right)$, the frequency spectra are computed following Wilson et al. (1991a) for the same four seasons as for the vertical wave number spectra. The average spectra along with their standard deviations were computed for the four seasons separately for the stratosphere and the mesosphere and are presented in Figs. 7a–d. The figures also show a power law spectral model with a slope of –5/3 for comparison. The spectra are found to be quite similar in shape for mesosphere and stratosphere but the former are two to three orders of magnitude greater. The computed spectra follow the model spectra for frequencies above $\sim 2\times10^{-4}$ Hz (periods 83 min) for all the seasons except for winter, for which it is $\sim 6\times10^{-4}$ Hz ($\sim$28 min). The constant of proportionality B_0 of the model spectrum takes values ranging from 0.1 in autumn to $\sim$1 in spring for the stratosphere and much higher values of $\sim$100 in the spring to $\sim$700 in the winter for the mesosphere. It is noted that the obtained value for autumn equinox needs further data base to conclude. The high standard deviations noted for autumn equinox are due to lower number of lidar observations used. The fewer lidar observations are due to the background the atmosphere conditions over the lidar site, such as the dominant south-west monsoon activities, passage of low-altitude clouds, precipitations and etc., which suspends the lidar observations.

It was shown by Nastrom et al. (1997) that a model for the ratio of kinetic to potential energy can be brought into agreement with the observed ratio if the power law index of

the frequency spectrum has a value of ∼–5/3 to –2. The observed spectra are found to follow the power spectral slope of –5/3 more closely for the stratosphere height region than for the mesosphere height region. Generally, the measured spectra follow the –5/3 spectra for the frequency range from $\sim 1.9\times10^{-4}$ to 8.75×10^{-4} Hz (periods ranging ∼20 to 90 min), except during winter, where it follows the frequency range from $\sim 5\times10^{-4}$ to 1.5×10^{-4} Hz (periods ranging ∼12 to 33 min). The spectra tend to level off or even show a positive slope for lower frequencies and a near negative slope for higher frequencies. The calculated mean ratio between the mesosphere and stratosphere spectral amplitude with model spectral slope (–5/3) shows a higher value for the mesosphere height region during summer, as well as for the stratosphere height region for autumn equinox. Using the zonal wind measurement at 86 km during summer at Poker Flat, Alaska, Carter and Balsley (1982) showed that for frequencies greater than the tidal band the spectral slope is very nearly –5/3. The lidar observations made during January 1989 at Biscarosse, Southern France, showed a spectral slope of about –2 for longer periods (3 1/2-h) and a significantly steeper slope for shorter periods, particularly for the stratosphere. These results are at variance with those presented here for the low latitude. Whiteway and Carswell (1995) never observed the growth of the wave amplitude beyond the marginal convective instability and the observations are consistent with the main hypothesis of the linear instability model of saturated GW spectra. Review work by Fritts and Alexander (2003) reported that the seasonal variation of gravity wave variations above 40 km exhibit a semiannual oscillation (SAO) at the equator. Also, the report pointed out that enhanced GW energy with vertical wavelengths of ∼2–10 km were observed at lower latitude (<30°), particularly due to strong convection, whereas at midlatitudes larger GW activity was seen more over continents than over oceans. They have also established that the spectral amplitudes may exceed saturation values at any altitude (especially in the mesosphere), where large vertical group velocities impose wave amplitude growth that is more rapid than the finite time required for instability dynamics to impose the wave amplitude constraints.

4.2 GW associated potential energy

Height profiles of potential energy associated with GW perturbations are computed using profiles of relative temperature fluctuations $\left(\frac{T'}{T_0}\right)$ obtained from the lidar data. It has been shown that the density and temperature fluctuations normalized to their mean values are about the same and either of them can be used to estimate the GW associated potential energy (Wilson et al., 1991 a, b; Whiteway and Carswell, 1994, 1995). The potential energy per unit mass is expressed as (Wilson et al., 1991a);

$$E_p = \frac{1}{2}\left(\frac{g}{N}\right)^2\left(\frac{T'}{T_0}\right)^2, \quad (6)$$

where N is the Brunt Väisälä frequency calculated from Eq. (1), T_0 and T' are the mean temperature and temperature perturbations.

The height profiles of mean potential energy are computed for all four seasons and presented in Figs. 8a–d. The potential energy increases with height gradually to about 50 J/kg at 60 km and rather rapidly above this height to reach a value of ∼200 J/kg at ∼70 km. The height variation for autumn equinox, unlike for the other seasons, shows two distinct peaks with values of ∼75 J/kg and ∼135 J/kg in the height ranges of 50–55 km and 60–65 km, respectively. The high standard deviation for autumn equinox may be due to less data used. Although, the figure shows an increase in potential energy, the lower mesosphere height region shows a seasonal dependence by displaying high perturbation during summer. It is also apparent from the figure that the summer profile showing more variability is in agreement with the case study result presented in Fig. 4a. The observed PE magnitude is found to be higher in comparison to the mid potential energy and high-latitude results (Wilson et al., 1991a, b). The reason for this may be addressed to the intense convective phenomena responsible for enhancing the GW activity occurring over the tropics (Fritts and Alexander, 2003).The seasonal difference in GW variations during spring and autumn equinox is partly consistent with the observed mesospheric temperature inversion in the height region of 70–80 and is reported more in detail by Sivakumar et al. (2001) for the samestation. On the other hand, it is in contrast to the mid-latitude observations by revealing maximum gravity wave activity during winter than equinox or summer (e.g. Wilson et al., 1991b; Allen and Vincent, 1995; Whiteway and Carswell, 1995; Yoshiki and Sato, 2000; Zink and Vincent, 2001). The above latitudinal dependence of the gravity wave seasonal behavior is also found to be in agreement with earlier reports using satellite data (Hirota, 1984; Fritts and vanZandt, 1993).

5 Summary and conclusion

The high-resolution (250 s and 300 m in time and height) Rayleigh lidar measurements made for 310 nights over March 1998 to December 2002 at Gadanki (13.5° N, 79.2° E) are used to study the gravity wave characteristics in the low-latitude middle atmosphere. The lidar observations revealed significant gravity wave activity over the entire observed height range of 30–70 km. The wave activity is seen to be distinctly different from stratosphere to mesosphere and for the different seasons. The obtained wave number spectra and frequency spectra illustrate the wave activity with the vertical wavelength of the order of 5–38 km and the time

period ranges from 20 min to 4 1/2 h. The wave number spectra are found to be quite different from the model spectra by recording high values than the stratosphere and mesosphere. Compared to the model spectrum, the computed wave number spectra are shallower at lower wave numbers and steeper at higher wave numbers, with the transition at $\sim 8.85 \times 10^{-4}$ cy/m. In magnitude, the computed spectra are greater by one to two orders of magnitude. Generally, the measured frequency spectra follow the –5/3 spectra for the frequency range from $\sim 1.9 \times 10^{-4}$ to 8.75×10^{-4} Hz (periods ranging $\sim$20 to 90 min). The observed spectral slopes associated with the vertical wave number and frequency spectra are found to differ significantly from the saturation spectral models, also in agreement with the earlier results from mid-latitudes (Shibata et al., 1988; Wilson et al., 1991b; Senft et al., 1993; Hostetler and Gardner, 1994; Nastrom et al., 1997; Nastrom and vanZandt, 2001). The mean potential energy shows increasing gravity wave activity with height and without much seasonal dependence.

Acknowledgements. The National Atmospheric Research Laboratory (NARL) is operated by the Department of Space with partial support from Council of Scientific & Industrial Research, Government of India. We would like to acknowledge with thanks the numerous contributions by our colleagues at NARL and Communications Research Laboratory, Japan in establishing and operating the lidar facility. Laboratoire de l'Atmosphère et des Cyclones (LACy) is supported by the French Centre National de la Recherche Scientifique (CNRS)/Institut National des Sciences de l'Univers (INSU) and the Conseil Régional de la Réunion.

Topical Editor U.-P. Hoppe thanks two referees for their help in evaluating this paper.

References

Alexander, M. J., Tsuda, T., and Vincent, R. A.: Latitudinal variations observed in gravity waves with short vertical wavelengths, J. Geophys. Res., 59, 1394–1404, 2002.

Allen, S. J., and Vincent, R.A.: Gravity wave activity in the lower atmosphere: Seasonal and latitudinal variations, J. Geophys. Res., 100, 1327–1350, 1995.

Beatty, T. J., Hostetler, C. A., and Gardner, C. S.: Lidar observations of gravity waves and their spectra near the Mesopause and Stratopause at Arecibo, J. Geophys. Res., 49, 472–497, 1992.

Booker, J. R. and Bretherton, F. P.: The critical layer for internal gravity waves in a shear flow, J. Fluid Mech., 27, 513–539, 1967.

Carter, D. A. and Balsley, B. B.: The summer wind filed between 80 and 93 km observed by the MST radar at Poket Flat, Alaska (65°N), J. Atmos. Sci., 39, 2905–2915, 1982.

Chanin, M. L. and Hauchecorne, A.: Lidar observation of gravity and tidal waves in the stratosphere and mesosphere, J. Geophys. Res., 86, 9715–9721, 1981.

Chanin, M. L. and Hauchecorne, A.: Lidar study of the structure and dynamics of the middle atmosphere, Indian J. Radio and Space Phys., 20, 1–11, 1991.

Dewan, E. M. and Good, R. E.: Saturation and the "universal" spectrum for vertical profiles of horizontal scalar winds in the stratosphere, J. Geophys. Res., 91, 2742–2748, 1986.

Dunkerton, T. J.: Wave transience in a compressible atmosphere, Part III: The saturation of internal gravity waves in the mesosphere, J. Atmos. Sci., 39, 1042–1051, 1982.

Fritts, D. C.: Gravity wave saturation in the middle atmosphere: A review of theory and observations, Rev. Geophys. Space Phys., 22, 275–308, 1984.

Fritts, D. C. and Rastogi, P. K.: Convective and dynamical instabilities due to gravity wave motions in the lower and middle atmosphere: Theory and observations, Radio Sci., 20, 1247–1277, 1985.

Fritts, D. C. and vanZandt, T. E.: Spectral estimates of gravity wave energy and momentum fluxes, 1. Energy dissipation, acceleration, and constraints, J. Atmos. Sci., 50, 3685–3694, 1993.

Fritts, D. C. and Alexander, M. J.: Gravity wave dynamics and effects in the middle atmosphere, Rev. Geophys., 41, 1/1003, 3, 1–64, 2003.

Fritts, D. C., Tsuda, T., Sato, T., Fukao, S., and Kato, S.: Observational evidence of a saturated gravity wave spectrum in the troposphere and lower stratosphere, J. Atmos. Sci., 45, 1741–1759, 1988.

Fritts, D. C., Tsuda, T., Vanzandt, T. E., Smith, S. A., Sato, T., Fukao, S., and Kato, S.: Study of velocity fluctuations in the lower atmosphere using the MU Radar, Part II : Momentum fluxes and energy densities., J. Atmos. Sci., 47, 51–66, 1990.

Gardner, C. S., Miller, M. S., and Liu, C. H.: Rayleigh lidar observations of gravity wave activity in the upper stratosphere at Urbana, Illonois, J. Atmos. Sci., 46, 1838–1853, 1989.

Gavrilov, N. M., Fukao, S., and Nakamura, T.: Gravity wave intensity and momentum fluxes in the mesosphere over Shigaraki, Japan (35°N ; 136° E) during 1987–1997, Ann. Geophys., 18, 834–843, 2000.

Hauchecorne, A. and Chanin, M. L.: Density and temperature profiles obtained by lidar between 35 and 70 km, Geophys. Res. Lett., 7, 565–568, 1980.

Hirota, I.: Climatology of gravity waves in the middle atmosphere, in Dynamics of the Middle Atmosphere, edited by: Holton, J. R. and Matsuno, T., Terra, Tokyo, 65, 1984.

Hostetler, C. A. and Gardner, C. S.: Observations of horizontal and vertical wave number spectra of gravity wave motions in the stratosphere and mesosphere over the mid-Pacific, J. Geophys. Res., 99, 1283–1302, 1994.

Lindzen, R. S.: Wave mean flow interaction in the upper atmosphere, Boundary Layer Meterol., 4, 327–343, 1973.

Marsh, A. K. P., Mitchell, N. J., and Thomas, L.: Lidar studies of stratospheric gravity-wave spectra, Planet. Space Sci., 39, 1541–1548, 1991.

Mitchell, N. J., Thomas, L., and Marsh, A. K. P.: Lidar observations of long period gravity waves in the stratosphere, Ann. Geophys., 9, 588–596, 1991.

McDonald, A. J., Thomas, L., and Wareing, D. F.: Night-to-night changes in the characteristics of gravity waves at stratospheric and lower-mesospheric heights, Ann. Geophys., 16, 229–237, 1998.

McIntyre, M. E.: An introduction to the generalized Lagrangian-mean description of wave, mean flow interactions, Pure Appl. Geophys., 118, 152–176, 1980.

Namboothiri, S. P., Tsuda, T., Tsutsumi, M., Nakamura, T., Nagasawa, C., and Abo, M.: Simultaneous observations of mesospheric gravity waves with the MU radar and a sodium lidar, J.

Geophys. Res., 101, 4057–4063, 1996.
Nastrom, G. D., vanZandt, T. E., and Warnock, J. M.: Vertical wavenumber spectra of wind and temperature from high-resolution balloon soundings over Illionis., J. Geophys. Res., 102, 6685–6701, 1997.
Nastrom, G. D., vanZandt, T. E.: Seasonal variability of the observed vertical wavenumber spectra of wind and temperature and the effect of prewhitening., J. Geophys. Res., 106, 14 369–14 375, 2001.
Röttger, J.: Structure and dynamics of the stratosphere and mesosphere revealed by VHF radar investigations, Pure Appl. Geophy., 118, 494–527, 1980.
Senft, D. C., Hostetler, C. A., and Gardner, C. S.: Characteristics of gravity wave activity and spectra in the upper stratosphere and upper mesosphere at Arecibo during early April 1989, J. Atmos. Terr. Phys., 55, 425–439, 1993.
Shibata, T., Ichimori, S., Narikiyo, T., and Maeda, M.: Spectral analysis of vertical temperature profiles observed by a lidar in the upper stratosphere and the lower mesosphere, J. Meterol. Soc., Jpn. 66, 1001–1005, 1988.
Sivakumar, V., Bhavanikumar, Y., Raghunath, K., Rao, P. B., Krishnaiah, M., Mizutani, K., Aoki, T., Yasui, M., and Itabe, T.: Lidar measurements of mesospheric temperature inversion at a low latitude, Ann. Geophys., 19, 1039–1044, 2001.
Sivakumar, V., Rao, P. B., and Krishnaiah, M.: Lidar studies of stratosphere and mesosphere thermal structure over a low latitude: Comparison with satellite and models., J. Geophys. Res., 108 (D11), 4342, doi: 10.1029/ 2002JD003029, 2003.
Smith, S. A., Fritts, D. C., and vanZandt, T. E.: Evidence of a saturated spectrum of atmospheric gravity waves, J. Atmos. Sci. 44, 1404–1410, 1987.
Tsuda, T., Inoue, T., Fritts, D. C., vanZandt, T. E., Kato, S., Sato, T., and Fukao, S.: MST radar observations of a saturated gravity wave spectrum, J. Atmos. Sci., 46, 2440–2447, 1989.
Vincent, R. A.: Gravity wave motions in the atmosphere, J. Atmos. Terr. Phys., 46, 119–128, 1984.
Whiteway, J. A. and Carswell, A. I.: Rayleigh Lidar observations of thermal structure and gravity wave activity in the High Arctic during a stratospheric warming, J. Atmos. Sci., 51, 3122–3136, 1994.
Whiteway, J. A. and Carswell, A. I.: Lidar observations of gravity wave activity in the upper stratosphere over Toronto, J. Geophys. Res., 100, 14 113–14 124, 1995.
Wilson, R., Hauchecorne, A., and Chanin, M. L.: Gravity wave spectra in the middle atmosphere as observed by Rayleigh lidar, J. Geophys. Res., 96, 5153–5167, 1991a.
Wilson, R., Hauchecorne, A., and Chanin, M. L.: Gravity waves in the middle atmosphere observed by Rayleigh lidar, Part 2: Climatology, J. Geophys. Res., 96, 5169–5183, 1991b.
Wu, Y. F. and Widdel, H. U.: Observational evidence of a saturated gravity wave spectrum in the mesosphere, J. Atmos. Terr. Phys., 51, 991–996, 1989.
Wu, Y. F. and Widdel, H. U.: Further study of a saturated gravity wave spectrum in the mesosphere, J. Geophys. Res., 96, 9263–9272, 1991.
Yoshiki, M. and Sato, K.: A statistical study of gravity waves in the polar regions based on operational radiosonde data, J. Geophys. Res., 105, 17 995–18 011, 2000.
Zink, F. and Vincent, R. A.: Wavelet analysis of stratospheric gravity wave packets over Macquarie Island, 1. wave parameters, J. Geophys. Res., 106, 10 275–10 288, 2001.